*Essential Readings in Light Metals: Electrode Technology for Aluminum Production.*
Edited by Alan Tomsett and John Johnson.

Light Metals — From ***Light Metals 1996***, Wayne Hale, Editor

# THE BEHAVIOUR OF NICKEL FERRITE CERMET MATERIALS AS INERT ANODES

Espen Olsen and Jomar Thonstad

Department of Electrochemistry
Norwegian Institute of Technology
N-7034 Trondheim, Norway

## Abstract

$NiFe_2O_4$-based cermet materials of varying compositions were fabricated using alternative techniques giving bodies with densities close to theoretical. The materials were used in electrolysis tests in a conventional electrolyte for 50 hours with continuous bath and metal sampling. Good performance of the electrodes was dependant on the formation of a stable oxide layer on the anode surface. Corrosion rates corresponding to the range of 0.12 - 0.20 cm/year were measured. The cathodically deposited aluminium was found to contain contaminants originating from the anode in the range of 3000 ppm. The anode dissolution process as well as the mass transfer of the contaminating species from the electrolyte into the metal cathode were investigated. The microstructure of the materials before and after testing was compared and very good characteristics were found, indicating that the anodes corroded in a controlled manner.

## Introduction

### General

As long as the Hall-Heroult process has been operated, the search for an inert anode material has been an issue in pursuit of new technology for the aluminium reduction process. In the present process, carbon anodes are used, the anode product being $CO_2$. With an inert anode, the cell reaction will be

$$Al_2O_3 = 2Al + \frac{3}{2}O_2 \qquad (1)$$

An inert anode should be: i) economically feasible, ii) exhibit a low corrosion rate iii) not contaminate the produced metal to any significant degree and iv) be a good electronic conductor. No material has yet been found which fulfil all these requirements.

As far back as in the 1930's Belyaev and Studentsov examined various oxides and ferrites with low solubilities in cryolitic melts as candidate materials for this purpose. No firm conclusions were drawn, but a number of materials were found to have a very low solubility in cryolitic melts. More recently, Aluminium Company of America (Alcoa) conducted, supported by US Department of Energy, a significant work on the use of ferrites [1]. Their effort ended in 1986, having developed a new cermet material consisting of a nickel ferrite-nickel oxide substrate containing Cu as a metal phase to give acceptable electrical conductivity. Battelle-PNL continued this work, but they were not able to reproduce the best results obtained by Alcoa with their original composition [2].

In the present study we have taken a new approach as we have applied different manufacturing methods to achieve a more fine-grained structure of $NiFe_2O_4$-cermets, and we have investigated the behaviour of different compositions during 50 hour electrolysis tests.

### Theory

All oxides have a finite solubility in cryolitic melts. The solubilities vary with a number of variables such as the cryolite ratio, CR (molar ratio $NaF/AlF_3$), the content of $Al_2O_3$ and the temperature. In our work we decided to concentrate on the behaviour of the anode materials as such, and consequently we chose a conventional Hall-Heroult electrolyte. A well behaving anode material should show a constant wear rate due to chemical dissolution in the electrolyte. From the anode substrate, the cations will dissolve and either leave the cell via the vapour phase, or they will be reduced by dissolved metal and enter the cathodically deposited aluminium pad via reaction (2):

$$Al + \frac{3}{n}M^{n+} = Al^{3+} + \frac{3}{n}M \qquad (2)$$

The rate of alloying is believed to be governed by a diffusion process as the reduced species are transferred through the boundary layer at the electrolyte/metal interface. This process is characterized by a mass transfer coefficient specific for each species. The flux of a contaminating species alloying into the cathode metal may be described by Equation (3) where J is the flux of the species entering the metal, k is the mass transfer coefficient of the species, $c_\infty$ is the steady state concentration in the electrolyte and $A_m$ is the area of the metal pad.

$$J = k \cdot c_\infty \cdot A_m \qquad (3)$$

As the process is dependent on the content of anode species in the electrolyte ($c_\infty$) one way to achieve low contamination of the deposited metal is to choose oxides of elements having low solubilities in the melt, or exhibiting a slow dissolution rate. Another approach is to find candidate materials having low mass transfer coefficients of the respective constituents into the deposited metal. The dissolution of oxides from the anode into the melt is usually assumed to be mass

transfer controlled, and the concentration of the anode constituents in the electrolyte may be described by Equation (5), which is derived from the general diffusional equation (Equation (4)) where $c_{sat}$ is the maximum solubility of the species in the electrolyte and r is the mass transfer coefficient or the rate of dissolution of the species from the anode into the electrolyte. V is the volume of the electrolyte.

$$J=r(c_{sat}-c_{\infty})A_a \quad (4)$$

$$c(t)=\frac{rc_{sat}A_a}{kA_m+rA_a}\left(1-e^{\frac{-(kA_m+rA_a)t}{V}}\right) \quad (5)$$

The scope of this work has been to manufacture materials of different compositions by varying the NiO content in the cermets; thereafter to study their corresponding performance regarding dissolution into the electrolyte and subsequent alloying into the aluminium cathode in 50 hour electrolysis tests with frequent bath and metal sampling. The reported results are part of a Ph.D study conducted at the Department of Electrochemistry at The Norwegian Institute of Technology.

## Fabrication of Materials

The powders were prepared from commercial grade chemicals. The suppliers and specifications were: $Fe_2O_3$: Harcros pigments, low silica type, Pigment grade, 99.3%, 5µm. $Fe_3O_4$: A/S Sydvaranger, low silica, 99.5%. NiO: Novamet, high purity green NiO, 99.98%, 5µm. Ni: Aremco Products, electronic grade, 99.9%, 3µm. Cu: Aremco Products, 99.8%, 1-5µm.

1200 g powder mix was blended for 18 hours in a stainless steel ball mill, dispersed in 1000 ml hexan using 10 g fish oil as dispersant. The mixture was dried and calcined at 1000°C for 2 hours in air to form the ferrite phase. Metal powders were added to the calcined powder and the mixture was again transferred to the ball mill and milled wet for an additional 18 hours before drying and screening through a 60 mesh screen. No binder was added to the powder, as the metal present in the powder was considered to be sufficiently ductile to achieve dense, machinable green bodies. Three different compositions were prepared with 0 wt% excess NiO, 17 wt% excess NiO and 23 wt% excess NiO in the ceramic phase respectively. The metal phase was modified compared to Alcoa's original composition by adding 3 wt% Ni to the metallic phase already constituting 17 wt% Cu. Ni has better wetting characteristics than Cu towards the oxide phases, and adding Ni should lead to smaller metal grains in the sintered samples. The composition of the individual phases in the materials after sintering is listed in Table 2. Stoichiometric $NiFe_2O_4$ contains 66.7 rel. at% Fe and 33.3 rel. at% Ni.

The powders were vibratory pre-compacted in latex moulds which were sealed and transferred to the cold isostatic press (CIP). The CIP pressure was 300 Mpa. The green body compaction grade was about 60% of theoretical. The sintering was conducted in a closed tube furnace. The maximum sintering temperature was 1350°C in Ar atmosphere. The same overall cycle as described by Weyand was used [3]. The sintered samples had a strong metallic lustre with occasional metal protrusions on the surface, indicating that the metal content was close to maximum without excessive metal bleed-out. Samples were prepared for characterization by SEM and X-Ray Diffraction (XRD). XRD showed no traces of uncalcined powder or foreign phases. The physical properties of the materials are given in Table 1. Reaction sintering, where the calcination process was incorporated in the sintering cycles, was also tried. This gave very dense materials, but with larger metal grains, which were considered unfavourable.

Table 1: Properties of sintered samples of different compositions. For 17 wt% excess NiO, sample (a) was prepared from powder produced as described above. (b) was prepared from a different batch of powder, (Rx) is reaction sintered material.

| wt % excess NiO | density [g/cm$^3$] | Theoretical density[g/cm$^3$] | % of theoretical |
|---|---|---|---|
| 0 | 5.06 | 5.82 | 86.9 |
| 17 (a) | 6.06 | 6.18 | 98.1 |
| 17 (b) | 6.12 | 6.18 | 99.0 |
| 17 (Rx) | 6.18 | 6.18 | 100 |
| 23 | 6.32 | 6.52 | 96.9 |

Table 2: Composition of the individual phases in the sintered materials as determined by X-ray Micro Analysis (XRMA).

| Material [excess wt%NiO] | phase | Fe [rel.at%] | Ni [rel.at%] | Cu [rel.at%] |
|---|---|---|---|---|
| 0 | metal | 5.4±0.2 | 37.1±0.7 | 57.6±0.9 |
| | $NiFe_2O_4$ | 77.1±0.6 | 22.0±0.5 | 0.8±0.3 |
| 17 | metal | 4.1±0.2 | 40.3±0.6 | 55.3±0.8 |
| | NiO | 24.6±0.3 | 75.3±0.7 | 0 |
| | $NiFe_2O_4$ | 75.0±0.5 | 25.0±0.5 | 0 |
| 23 | metal | 4.4±0.2 | 32.6±0.6 | 62.7±0.9 |
| | NiO | 16.7±0.3 | 82.3±0.8 | 0 |
| | $NiFe_2O_4$ | 71.0±0.6 | 27.3±0.5 | 1.0±0.3 |

The electrical conductivities at 980°C were 70 S/cm and 90 S/cm for the materials containing 17 wt% and 23 wt% excess NiO respectively. These materials showed semiconducting behaviour in the temperature range of interest. For the all-ferrite material with no excess NiO, the conductivity varied from 250 S/cm at 650°C to 30 S/cm at 1000°C, exhibiting metallic type conductivity in this temperature range. These results will be reported more extensively in later publications.

## Electrolysis Tests

The cell used in the 50 hour electrolysis tests is sketched in Figure 1. It consisted of a graphite crucible lined with a thick-walled sintered alumina tube. The inner diameter of the cell was 100 mm. On the bottom of the cell was placed a rectangular piece (5x5 cm) of $TiB_2$-graphite composite (5 wt% C, Great Lakes Carbon) to serve as cathode. The rest of the cell bottom was insulated with a disk of 10

mm thick sintered alumina. The crucible was polarized cathodically through a 6 mm inconel rod. The anodic current was provided through a similar inconel rod attached to the anode with Cu-based cement. The anode current lead was protected from corrosion with a sintered alumina tube. A cylindrical anode with height 8 cm and diameter 4 cm was used.

The cell contained a total of 2300 g electrolyte of CR 2.2 ($NaF/AlF_3$ molar ratio). 5 wt% $CaF_2$ was added and the alumina concentration was kept close to saturation (8 wt%) throughout the tests. The temperature was 960°C.

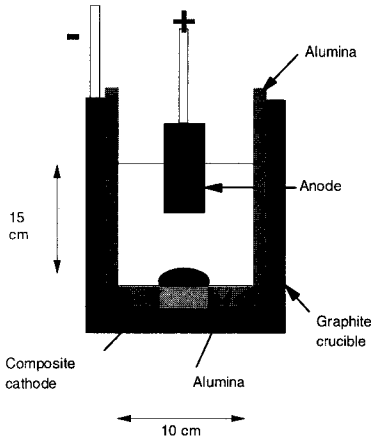


Figure 1: Electrochemical cell used in the 50 hour experiments.

Bath samples were taken to determine the level of anode constituents in the melt during the tests. Change in the concentration in the initial phase was considered important in the sense that it could be used for determination of the mass transfer coefficient of the various species from the anode to the bath. Bath samples were, therefore, taken at 5 minute intervals for the first 30 minutes of the tests, then every 10 minutes for the next 30 minutes. Preliminary tests had shown that the electrolyte reached a steady state of contamination with respect to species originating from the anode after about 60 minutes. Later in the tests, the samples were taken at random intervals in conjunction with metal sampling. The bath samples were analyzed using XRF spectroscopy. The metal sampling was made at irregular intervals throughout the tests, using a quarz tube which was lowered into the cathodic metal pad. The metal samples were dissolved in 100 ml concentrated HCl and analyzed using an Argon ICP spectrometer.

The cell was operated for 50 hours with an anodic current of 15A. The total immersed anode surface area was 75 $cm^2$. Current distribution calculations showed that about 40% of the current was conducted through the horizontal, bottom part of the anode, implying that the current density here was 0.5 $A/cm^2$. The cell voltage was very stable during the tests with occasional disturbances in conjunction with the metal sampling.

## Results and Discussion

### Contamination of the electrolyte

The contamination of the electrolyte was studied both in the initial part of the tests and over a longer time span. It was assumed that the anode would exhibit a wear rate caused by steady state chemical dissolution rather than an uncontrolled corrosion process. In the initial stage of the tests the bath contamination is expected to rise rapidly to a steady state value following a simple mass transfer controlled mechanism as described by Equation (4). The steady state value of the concentration of the contaminating species, $c_\infty$ will be a function of the maximium solubility of the species in the electrolyte, $c_{sat}$, the rate of alloying of the species into the aluminium, $kA_m$, and the rate of dissolution of the anode material, $rA_a$. Possible evaporation of the contaminant was neglected since it was assumed to be of minor importance. As time proceeds, the time dependent part of Equation (5) becomes negligible and the steady state contamination of the bath is given by Equation (6). In this equation, r is the dissolution rate constant of the anode, $A_a$ is the active surface area of the anode, k is the mass transfer coefficient of the alloying of the species into the cathode, and $A_m$ is the cathode surface area.

$$c_\infty = \frac{rc_{sat}A_a}{kA_m + rA_a} \qquad (6)$$

For a mass transfer controlled process, the rate of dissolution of a gas evolving, oxidic anode will be much more rapid than the alloying of the species into the cathodically deposited metal. It may therefore be assumed that the value of $c_\infty$ should be close to $c_{sat}$. Experimental data for the contamination of the electrolyte versus time for the anode species is plotted in Figure 2 a, b and c for the three tested materials respectively.

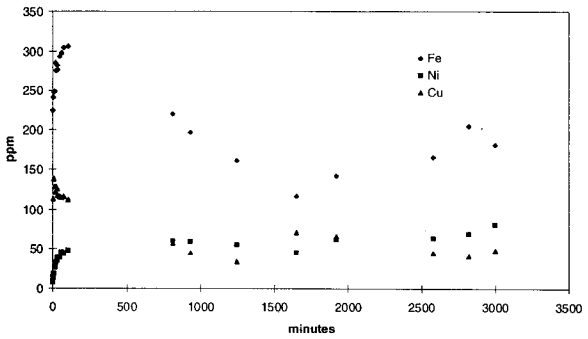


Figure 2a: Bath contamination versus time. All ferrite material (0 % excess NiO) in the ceramic phase.

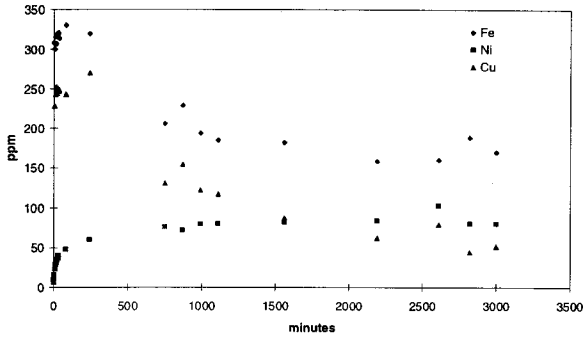


Figure 2b: Bath contamination versus time. 17 wt% excess NiO in the ceramic phase.

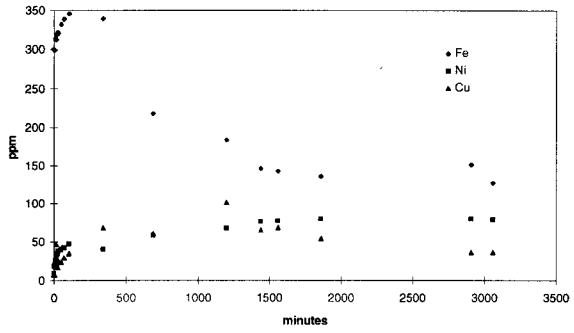


Figure 2c: Bath contamination versus time. 23 wt% excess NiO.

As can be seen from the figures, the levels of contamination do indeed reach a stable value. The levels of Fe and Cu, however, seem to follow the expected increasing trend early in the tests and thereafter to decrease to stable values which are well below saturation [4]. This implies that the rate of anode dissolution is rapid in the beginning of the tests, slowing down and reaching a stable value where the rate of species lost from the bath is equal to the rate dissolving from the anode. It is interesting to note that for these species, the level of contamination of the bath is considerably below saturation [4].

Nickel seems to behave as expected by increasing to a stable value with no subsequent decrease. DeYoung [4] have found that the saturation level of Ni in similar melts is around 70-80 ppm. In the present study, a steady state level of 50 ppm is found, indicating that the steady-state value is below saturation. Only minor differences were observed between the tested anode compositions, the levels of Ni and Cu being somewhat lower for the material without excess NiO, and the Fe level being lower for the material containing 23 wt% excess NiO.

The time dependent behaviour of the contamination early in the tests was studied to determine the dissolution rate of the anode materials. The data were curve fitted to the model described by Equation (5) with the time independent part being considered a constant denoted by $c_\infty$. as described by Equation (6). Simulated curves for the individual species together with the actual measured values are shown in Figures 3 a, b and c. The corresponding curve fitted parameters are listed in Tables 3 a,b and c respectively. In the tables, $c_0$ denotes the initial contamination of the species in the electrolyte used in the simulations.

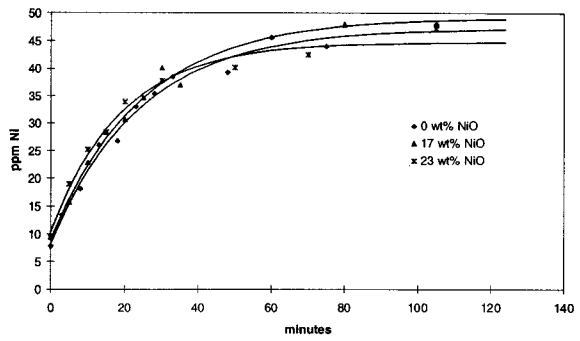


Figure 3a: Ni dissolution from the anode with best fit curves using Equation (5).

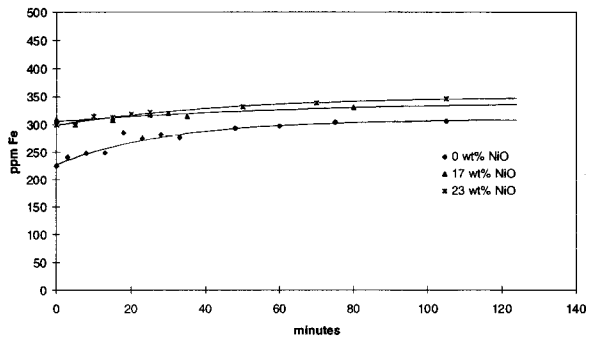


Figure 3b: Fe dissolution from the anode with best fit curves using Equation (5).

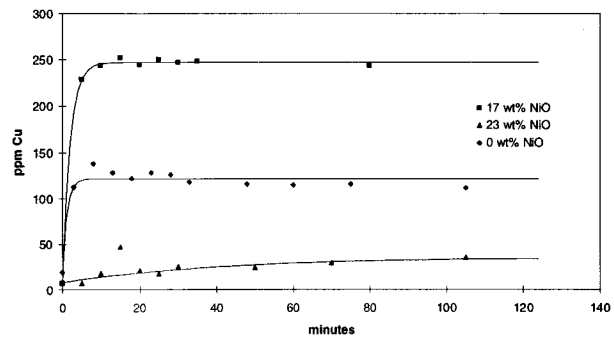


Figure 3c: Cu dissolution from the anode with best fit curves using Equation (5).

able 3a: Curve fitting parameters for Ni.

| Material [wt% NiO] | $c_\infty$ [ppm] | $c_0$ [ppm] | r [m/s] |
|---|---|---|---|
| 0 | 47.3 | 8.2 | $1.08 \cdot 10^{-4}$ |
| 17 | 49.2 | 8.9 | $0.92 \cdot 10^{-4}$ |
| 23 | 44.8 | 10.3 | $1.22 \cdot 10^{-4}$ |

Table 3b: Curve fitting parameters for Fe.

| Material [wt% NiO] | $c_\infty$ [ppm] | $c_0$ [ppm] | r [m/s] |
|---|---|---|---|
| 0 | 309.5 | 227.1 | $8.68 \cdot 10^{-5}$ |
| 17 | 342.7 | 305.6 | $3.05 \cdot 10^{-5}$ |
| 23 | 350.8 | 294.4 | $4.93 \cdot 10^{-5}$ |

Table 3c: Curve fitting parameters for Cu.

| Material [wt% NiO] | $c_\infty$ [ppm] | $c_0$ [ppm] | r [m/s] |
|---|---|---|---|
| 0 | 121.9 | 18.9 | $2.20 \cdot 10^{-3}$ |
| 17 | 247.0 | 7.0 | $1.1 \cdot 10^{-3}$ |
| 23 | 35.7 | 8.1 | $5.49 \cdot 10^{-6}$ |

The dissolution of Ni is very similar for all the materials and the simulated curves suggest that the mass transfer coefficients for Ni from the anode to the electrolyte is in the vicinity of $1 \cdot 10^{-4}$ m/s. This value is a factor of 2 higher than previously reported by Weyand et al. [1]. The behaviour of Fe is somewhat masked by the high initial content of iron in the melt, but the simulated curves seem to describe the behaviour adequately. The initial contamination of Fe in the test with the all ferrite anode material was lower than in the two other tests, as evidenced in the figure. This is ascribed to variations in the Fe content in natural cryolite. The final steady state concentration $c_\infty$ of Fe is about 300 ppm in all the tests, the all ferrite material approaching a somewhat lower value of 280 ppm. DeYoung found the maximum solubility of Fe in a similar melt to be 1000 ppm [4]. Table 3b shows that the mass transfer coefficient for Fe is higher for the material without excess NiO. The formation of $NiFe_2O_4$ from NiO and $Fe_2O_3$ has a Gibbs energy of -16.75 kJ/mol (Equation (7)).

$$Fe_2O_3 + NiO = NiFe_2O_4 \qquad (7)$$

$$K = \frac{a_{NiFe_2O_4}}{a_{NiO} \cdot a_{Fe_2O_3}} \qquad (8)$$

This implies that in the presence of excess NiO ($a_{NiO}=1$), the activity of $Fe_2O_3$ according to Equation (8), is 0.2. With no excess NiO and an NiO activity less than unity, the activity of $Fe_2O_3$ is higher, which in its turn might lead to a higher rate of dissolution of Fe from the anode into the melt.

The behaviour of Cu is different as the metallic phase is believed not to be electrochemically stable during polarization, leading to anodic dissolution of the metal grains exposed to the electrolyte. This is evidenced in the significantly higher values of $r_{Cu}$. It is doubtful whether the simple model used in the curve fitting describes this process well. Tarcy proposed that Cu dissolves by first forming copper oxides which then dissolve in the melt [5]. Copper oxides have, however, not been found in XRD measurements [6], and the rapid rise of the Cu content in the electrolyte suggests that the dissolution of the metallic copper phase does not involve initial formation of copper oxides.

The behaviour of the Cu and Fe species after the initial dissolution period was curious as the concentrations both dropped to about 50% of the initial seemingly stable steady state values. This behaviour might be due to a concentration gradient from the anode to the cathode being formed after a certain time in the more stagnant lower part of the cell as the species are transferred towards the cathode. After the cell had cooled down, it was cut in half and a greyish layer of electrolyte, more dense than in the area around the anode and about 1 cm thick, was found above the cathode where gas induced circulation had been ineffective. The fact that the electrolyte is not close to saturation with respect to contaminants is interesting, as this implies that after the initial period, the rate of dissolution of species from the oxidic anode is of the same order as the mass transfer rate of species into the cathode.

Metal Contamination

Apart from the original work by Alcoa, few laboratory studies have been conducted for such a long time that metal sampling during the tests could give meaningful data [7]. A pilot cell test conducted at Reynolds Metals inc. Manufacturing Tchnology, showed highly varying rates of metal contamination [8]. In a cell operating at steady state conditions, impurities should be entering the cathodically deposited aluminium at a constant rate according to Equation (9).

$$J = c_\infty k A_m \qquad (9)$$

If any loss of anode constituents from the bath to the vapour phase is neglected, the rate of alloying of the species into the metal should relate directly to the corrosion rate of the anode. The cathodic process can be viewed as a separate process, dependent only on the contamination in the electrolyte $c_\infty$, the mass transfer coefficient k and the area of the metal pad.

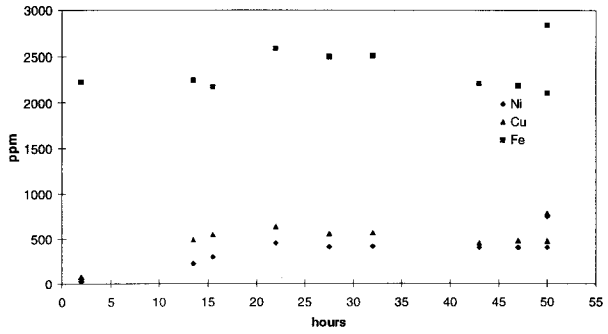


Figure 4a: Metal contamination of anode constituents. The anode material contained no excess NiO. The higher values at 50 hours are samples taken after cell cool down.

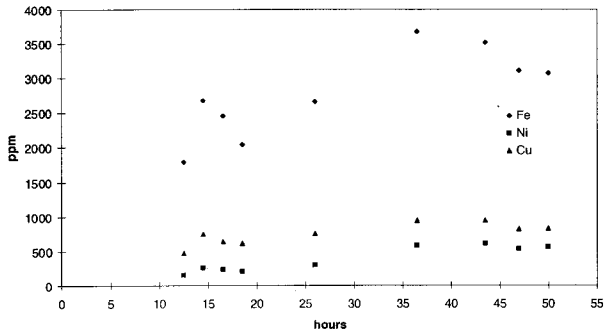


Figure 4b: Metal contamination of anode constituents. The anode material contained 17 wt% excess NiO.

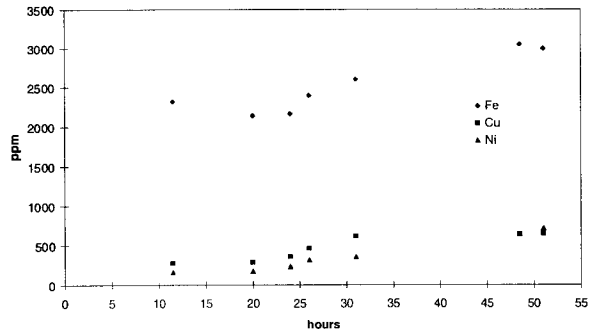


Figure 4c: Metal contamination of anode constituents. The anode material contained 23 wt% excess NiO.

In this study, metal samples were taken at irregular intervals during the tests to study the time dependent rate of alloying into the metal. If a linear behaviour of the amount of contaminating species entering the metal were found, it would be indicative of stable operation where the anode corrosion equalled the amount of anode constituents entering the metal. ICP analysis data for the contamination of the produced metal are found in Figures 4a, b and c.

These figures illustrate the major problem with oxidic inert anodes. A certain amount of impurities will eventually find its way into the deposited metal. While the total sum of impurities is as low as 0.3 wt%, and consequently may seem to be acceptable as primary metal, the individual contents of Ni and Cu are above the acceptable limits. The all ferrite material shows a lower contamination of all constituents, and this material also shows fairly stable values after 24 hours of electolysis, indicating stable operation where the anode corrodes in a controlled manner.

Considerable quantities of metal were removed from the cell due to sampling, and to study the rate of alloying, the total amount of anode constituents having entered the metal was calculated. These data are plotted versus time in Figures 5a, b and c. The results are summarized in Table 4.

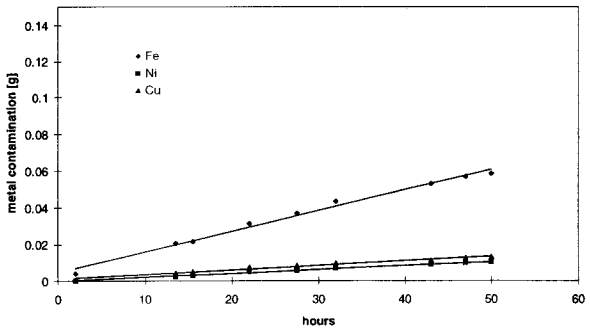


Figure 5a: The rate of alloying of anode cations into the deposited metal versus time. The anode material contained no excess NiO. The lines are drawn assuming linear behaviour.

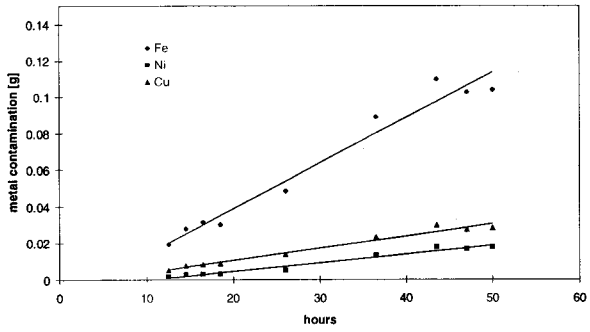


Figure 5b: The rate of alloying of anode constituents into the deposited metal versus time. The anode material contained 17 wt% excess NiO.

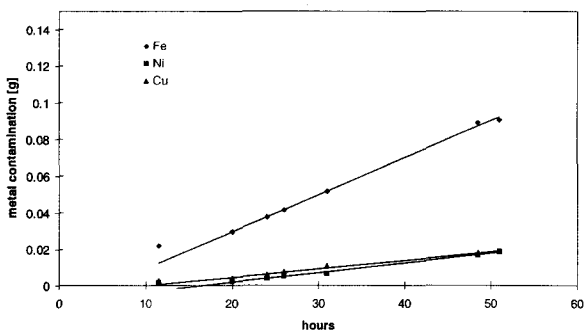


Figure 5c: The rate of alloying of anode constituents into the deposited metal versus time. The anode material contained 17 wt% excess NiO.

Table 4: Rate of anode constituents entering the deposited metal for $NiFe_2O_4$-based anodes of different compositions. A linear process as described by Equation (9) is assumed.

| Material | Fe [g/s] | Ni [g/s] | Cu [g/s] |
|---|---|---|---|
| 0 wt% NiO | $3.11 \cdot 10^{-7}$ | $0.58 \cdot 10^{-7}$ | $0.70 \cdot 10^{-7}$ |
| 17 wt% NiO | $6.92 \cdot 10^{-7}$ | $1.29 \cdot 10^{-7}$ | $1.84 \cdot 10^{-7}$ |
| 23 wt% NiO | $5.58 \cdot 10^{-7}$ | $1.49 \cdot 10^{-7}$ | $1.31 \cdot 10^{-7}$ |

The data indicate clearly that the anode constituents enter the metal pad at a constant rate. The two materials containing excess amounts of NiO show very similar characteristics, while contaminants from the all-ferrite material enter the metal at a lower rate. This is difficult to explain since the alloying process should only be dependent on the contamination levels in the electrolyte, which is not very different for these materials. A possible explanation is that at the applied temperature, the all-ferrite material has a considerably lower electrical conductivity. This will cause more current to pass through the sides of the anode, resulting in less convection in the lower part of the cell. The mass transfer coefficient is a function of the diffusion length through the stagnant boundary layer over the metal pad, and an increase in the thickness of the layer from 1 to 2 cm can explain the observed behaviour as the mass transfer coefficient is related to the diffusion constant for the actual element, D and the diffusional length, l according to Equation (10).

$$k = \frac{D}{l} \qquad \textbf{(10)}$$

The calculated mass transfer coefficients are listed in Table 7. The individual ratios between the mass transfer coefficients were also calculated. In these values individual differences in variables such as convection will be cancelled out. The ratios are given in Table 8.

Table 7: Mass transfer coefficients for the different anode species into the deposited metal.

| Material | $k_{Fe}$ [m/s] | $k_{Ni}$ [m/s] | $k_{Cu}$ [m/s] |
|---|---|---|---|
| 0 wt% NiO | $2.99 \cdot 10^{-7}$ | $1.59 \cdot 10^{-7}$ | $2.86 \cdot 10^{-7}$ |
| 17 wt% NiO | $6.65 \cdot 10^{-7}$ | $2.64 \cdot 10^{-7}$ | $6.00 \cdot 10^{-7}$ |
| 23 wt% NiO | $6.52 \cdot 10^{-7}$ | $3.04 \cdot 10^{-7}$ | $5.34 \cdot 10^{-7}$ |

Table 8: The ratios between the mass transfer coefficients in Table 7

| Material | $k_{Fe}/k_{Nii}$ | $k_{Fe}/k_{Cu}$ | $k_{Cu}/k_{Ni}$ |
|---|---|---|---|
| 0 wt% NiO | 1.88 | 1.05 | 1.80 |
| 17 wt% NiO | 2.52 | 1.11 | 2.27 |
| 23 wt% NiO | 2.14 | 1.22 | 1.76 |

As can be seen from Table 7, the mass transfer coefficients in the test with the all-ferrite anode (0 wt% excess NiO) are lower than the others by a factor of about two. This suggests that there is indeed an external factor which have influenced the mass transfer. For the two other materials, the values are quite similar the difference being no more than 15%.

The values in Table 8 show good agreement, and a number of conclusions can be drawn from the data. Fe and Cu seem to enter the metal at about the same rate, Fe showing a slightly higher rate. Ni, on the other hand, has a significantly lower mass transfer coefficient, being about half of that for Fe and Cu. This suggests that a Ni-based material as NiO should be further investigated as a candidate for an inert anode. When considering the mass transfer coefficients measured in these tests in general, they appear to be quite low compared to a typical value of $10^{-5}$ m/s, which is often encountered in molten salts.

Material Behaviour

After being left to cool down above the electrolyte, the anodes were removed from the cell. No attempt was made to measure the densitiy of the anode after electrolysis, because of adhering bath and alumina from the feed. Samples were cut from the bottom part of the anode to investigate the horizontal surface, since it was expected that it would exhibit the most severe corrosion. The samples were prepared for SEM by moulding in epoxy, and polished for XRMA analysis. SEM pictures are found in Figures 6a, b and c. For each composition, pictures were taken at the cermet electrolyte boundary and in the interior of the anode. The materials seemed to have behaved very well as there were no visible structural changes when going from the undisturbed interior of the electrode to the surface. On all anodes a dense all-oxide layer was formed on the surface, being about 50μm thick.

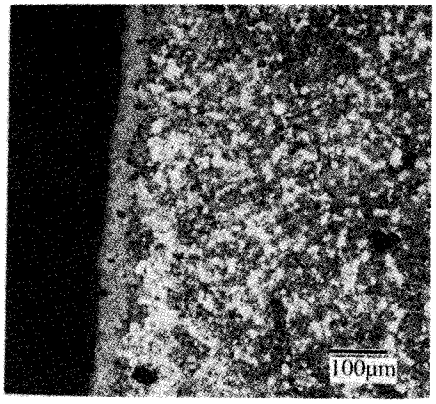


Figure 6a: Material containing no excess NiO, 100x

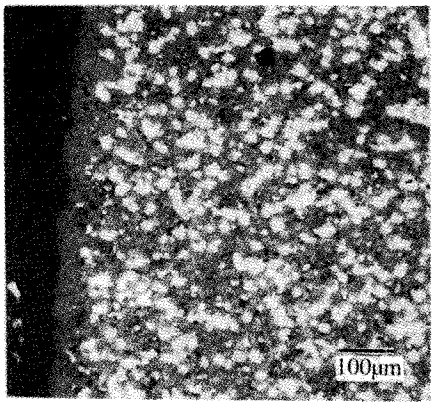


Figure 6b: Material containing 17 wt% excess NiO, 100x

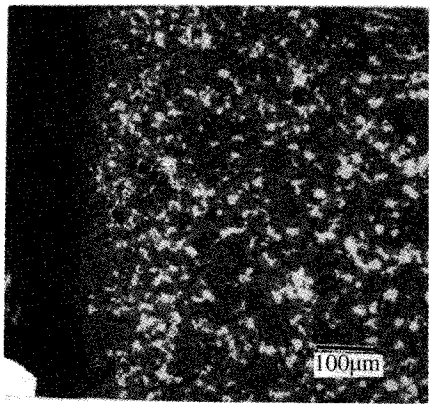


Figure 6c: Material containing 23 wt% excess NiO. 100x

Quantitative XRMA analyses

The polished samples were analyzed by XRMA using a quantitative energy dispersive spectrometer (EDS) connected to the SEM. The compositions of the individual phases were examined for each anode as a function of position relative to the anode-electrolyte interface. Individual grains were analyzed quantitatively with respect to the content of the metal cations, i.e. oxygen was exluded. The equipment used was fitted with a Be window which prevented analysis of the oxygen content in the various grains. The results were normalized to 100 at%, which may mask contamination of the phases with regards to species other than the ones analyzed. However, no peaks from such other elements were found in the X-ray spectra. All the different phases were analyzed in three positions, i.e. in the deep interior >2cm from the interface, at 200 µm from the interface and as close to the interface as possible.

No compositional changes were found to have taken place neither in the $NiFe_2O_4$ nor in the NiO phase when going from the interior to immediatly inside of the metal-electrolyte interface. The Ni content in the metallic phase decreased systematically from the interior of the anode to the interface. This was found only in used anodes, as this trend was not observed in unused reference specimens. The all-oxide reaction layer at the surface of the anodes was investigated, and the results are listed in Table 9. The quantitative analysis data for the metal phase are listed in Table 10.

Table 9: XRMA analyses of the reaction layer at the anode-electrolyte interface in the different anode samples.

| Material [excess wt% NiO] | Al [rel. at%] | Fe [rel. at%] | Ni [rel. at%] | Cu [rel. at%] |
|---|---|---|---|---|
| 0 | 2.9±0.1 | 67.9±0.9 | 25.6±0.4 | 4.5±0.3 |
| 17 | 2.5±0.2 | 68.2±0.5 | 27.1±0.5 | 2.1±0.3 |
| 23 | 1.3±0.1 | 68.5±0.6 | 29.6±0.5 | 0.6±0.2 |

Table 10: XRMA analyses of the metal phase in different parts of the anode samples.

| Material [wt% NiO] | Position rel. to interface | Al [rel. at%] | Fe [rel. at%] | Ni [rel. at%] | Cu [rel. at%] |
|---|---|---|---|---|---|
| 0 | interior | 0 | 8.4±0.2 | 38.8±0.5 | 52.1±0.7 |
| | 200µm | 1.1±0.2 | 7.6±0.2 | 24.2±0.4 | 67.0±0.8 |
| | 20µm | 1.0±0.1 | 5.2±0.2 | 22.4±0.4 | 71.3±0.8 |
| | | | | | |
| 17 | interior | 0 | 5.0±0.2 | 39.8±0.6 | 56.6±0.8 |
| | 200µm | 0 | 3.7±0.2 | 22.7±0.5 | 73.4±0.9 |
| | 20µm | 0 | 4.2±0.2 | 20.6±0.5 | 75.1±0.9 |
| | | | | | |
| 23 | interior | 0 | 2.1±0.1 | 36.0±0.5 | 61.4±0.7 |
| | 200µm | 0 | 3.8±0.2 | 21.0±0.5 | 75.2±0.9 |
| | 20µm | 0 | 5.0±0.2 | 21.5±0.4 | 73.6±0.9 |

The metallic phase is not electrochemically stable when polarized anodically in the electrolyte. As mentioned above, it has been suggested that the Cu-rich metallic phase might be protected by a stable copper oxide layer being formed on the surface [5]. This has not been observed in previous studies involving XRD measurements [6], and it is more likely that exposed metal grains dissolve anodically until a metal free oxidic layer has been formed on the surface, protecting the metal grains in the underlying substrate. The metal phase exhibits a gradient from the interior to the surface of the anodes with regard to the Ni content. This has also been observed in short term tests where the Ni-depleted region was found to extend 100-200 µm into the anode substrate. The data suggests that Ni is transferred preferentially to the electrolyte through the structure as the compositions of both the oxidic phases do not exhibit any significant changes.

The all-oxide reaction layer is of importance in the sense that apart from Fe and Ni, it contained small amounts of both Al and Cu. This was observed for all the materials. The Fe/Ni ratio suggests that this layer constitutes a ferrite-like phase, and the Cu and Al components

may, as Fe also does, occupy different lattice positions. At the surface the oxygen partial pressure is 1 atm, and it is reasonable to assume that these species occur in their highest valence states, i.e. Al (III) and Cu (II). These elements would then occupy different positions, Al entering the Fe positions and Cu entering the Ni positions respectively. In an earlier work, $FeAl_2O_4$ was found in small amounts at the surface of cermet anodes after 4 hours of electrolysis [6]. It is reasonable to assume that this is the case also here.

It has previously been assumed that cermet anodes are corroding via a mass transport controlled mechanism while polarized anodically in cryolite melts [9]. The formation of an oxidic reaction layer at the surface of the anodes tested in this work indicates that this might not be the case. If the corrosion process is governed by reaction control, it will have serious implications on the understanding of the behaviour of inert cermet anodes in cryolitic melts.

## Conclusions

- Dense nickel ferrite based cermets were manufactured having smaller grain size than the material previously made by Alcoa .
- Very low corrosion rates corresponding to 0.12 - 0.20 cm/year were measured in 50 hour tests.
- An all-oxide reaction layer was formed on all the materials tested. The layer was ~50μm thick and it prevented preferential attack of the metal grains in the substrate.
- Constant concentrations of anode constituents in the electrolyte were reached after 24 hours of electrolysis. The contents of Fe, Ni and Cu originating from the anode were below the saturation values for the corresponding oxides
- The transfer of species from the anode to the electrolyte was characterized by mass transfer coefficients at the order of $10^{-4}$ m/s for Fe and Ni, and $10^{-3}$ m/s for Cu in the start up period of the tests.
- The alloying of species from the electrolyte into the cathodically deposited metal was linear with time, and the process was characterized by mass transfer coefficients of the order of $10^{-7}$ m/s.
- The steady state contamination of anode constituents in the deposited metal was in the range of 2200-3000 ppm Fe, 400-700 ppm Cu and 400-600 ppm Ni.
- Ni has a significantly lower mass transfer coefficient into the metal than Fe and Cu. This calls for further work with nickel based materials.

## Acknowledgements

The authors gratefully acknowledge financial support from the Norwegian Research Council and the Norwegian aluminium industry. The Elkem Materials Company and in particular Dr. Raymond Cutler have been of invaluable help providing new ideas for the processing of the cermets.

## References

1. Weyand J.D., DeYoung D.H., Ray S.P., Tarcy G.P., Baker F.W., "Inert Anodes for Aluminium Smelting, Final Report", (Aluminium Company of America, Alcoa Laboratories, Alcoa Center, 1986). DOE No. DOE/CS/40158-20

2. Strachan D.M., Koski O. H., Morgan L.G., Westerman R.E., Peterson R. D., Richards N.E., Taberaux A.T.,"Results of 100 hour Electrolysis Test of a Cermet Anode: Materials Aspects", Light Metals, 1990, pp 395-401.

3. Weyand J.D., "Manufacturing Process Used for the Production of Inert Anodes", Light Metals, 1986, pp 321-339.

4. De Young D.H., "Solubilities of Oxides for Inert Anodes in Cryolite-based Melts", Light Metals, 1986, pp 209-308.

5. Tarcy G.P., "Corrosion and Passivation of Inert Anodes in Cryolite-Type Electrolytes", Light Metals, 1986, pp 309-320.

6. Olsen E., "Karakterisering av Cu-dopet $NiFe_2O_4$ som inert anodemateriale i aluminiumselektrolysen", Graduation thesis, Norwegian Inst. of Technology, 1991.

7. Baker F.W., Rolf R.C., "Hall Cell Operation with Inert Anodes", Light Metals, 1986, pp 275-286.

8. Peterson R.D., Richards N.E., Taberaux A.T., Strachan D.M., Koski O. H., Morgan L.G., Westerman R.E., "Results of 100 hour Electrolysis Test of a Cermet Anode, Operational Results and Industry Perspectives", Light Metals, 1990, pp 385-393.

9. Evans J.W., Keller R., "Factors affecting the life of inert anodes for aluminium electrolysis", Extended Abstracts, Fall Meeting of The Electrochemical Society, San Diego, USA, 1986, pp 966-967.